THE JOURNAL OF PHYSICAL CHEMISTRY C

Article

pubs.acs.org/JPCC

Interatomic Potential of Li−Mn−O and Molecular Dynamics Simulations on Li Diffusion in Spinel $Li_{1-x}Mn_2O_4$

Eunkoo Lee,[†] Kwang-Ryeol Lee,[‡] and Byeong-Joo Lee*[,†]

[†]Department of Materials Science and Engineering, Pohang University of Science and Technology (POSTECH), Pohang 37673, Republic of Korea

[‡]Computational Science Center, Korea Institute of Science and Technology, Seoul 02792, Republic of Korea

Supporting Information

ABSTRACT: An interatomic potential of the Li−Mn−O ternary system has been developed on the basis of the second-nearest-neighbor modified embedded-atom method (2NN MEAM) formalism combined with a charge equilibration (Qeq) concept. The potential reproduces fundamental physical properties (structural, elastic, thermodynamic and migration properties) of various compounds well, including lithium oxides, manganese oxides, and lithium manganese ternary oxides. Through molecular dynamics (MD) simulations using the developed potential, lithium diffusion properties (activation energy for lithium migration and diffusion coefficient) in spinel $Li_{1-x}Mn_2O_4$ are also reproduced in good agreement with experiments. We have found that the effect of the lithium vacancy concentration is marginal on the activation energy for lithium diffusion in the $Li_{1-x}Mn_2O_4$ cathode, but it is significant in the lithium diffusion coefficient. The potential can be further utilized for atomistic simulations of various materials phenomena (phase transitions, defect formation, lithiation/delithiation, etc.) in LIB cathode materials.

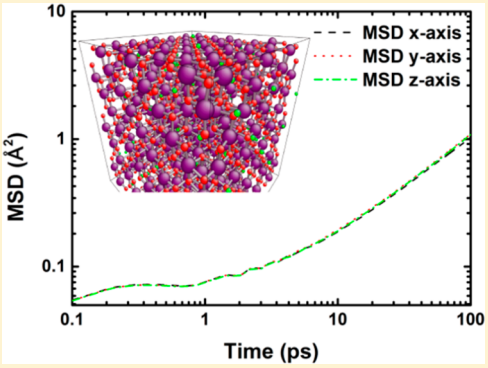

1. INTRODUCTION

From the early stages of battery development, $LiCoO_2$ has been the most widely used cathode material for lithium ion batteries (LIB) due to its characteristics of high voltage, fast Li ion migration, and high capacity.[1] Despite the successful commercialization of $LiCoO_2$ as a cathode material over the past 20 years, searches for a replacement material with low Co content have been extensively conducted due to high materials cost, toxicity of Co, and performance degradation during overcharge.[2,3] The number of possible compounds and doping elements is almost limitless, making it laborious and inefficient to search for new cathode materials. Moreover, important materials phenomena of cathode materials, such as diffusion, phase transition, defect formation, and lithiation/delithiation, are atomic-scale behavior that is difficult to observe experimentally. Therefore, in order to develop LIB cathode materials, it is necessary to have an effective and reliable approach to investigate such materials phenomena. In this case, computational approaches can provide useful insight and guidance into materials phenomena that are rather difficult to examine directly through experimental methods. Among such approaches, first-principles density functional theory (DFT) calculations provide the most reliable information on (sub)-atomic-scale physical properties. However, due to limits of size (or the number of atoms), it is often not possible to investigate material behaviors using only DFT calculations. Another approach is large-scale atomistic simulation using a (semi)-empirical interatomic potential model. This can be an effective method to investigate the aforementioned materials phenomena for LIB cathode materials on a larger scale.

However, even with the clear necessity of large-scale atomistic simulation, relatively few efforts have been made for the LIB cathode materials. We believe that this is not because the atomistic simulation is not important, but because it has been difficult to develop suitable interatomic potential models (and parametrization) for the LIB cathode materials. The materials system for LIB cathode materials consists mainly of multicomponent lithium transition-metal oxides (Li−TM−O). Therefore, the potential model should be able to simultaneously cover various bonding natures, such as metallic, covalent, and ionic bonds in the material under consideration. In addition, the model should be able to describe realistically that the charge state of atoms can vary dynamically during the charge/discharge process due to changes in crystal structure, lithium concentration, and oxidation states of transition metals, etc. For these reasons, a many-body potential coupled with a variable charge model is appropriate for covering the complicated LIB cathode materials system. Most previous studies, however, have used a pairwise-type potential with a fixed or partially variable charge model.[4−12] The classical pairwise potential model is not suitable to cover the wide range of materials systems associated with LIB cathode materials, and

Received: March 22, 2017
Revised: May 16, 2017
Published: June 6, 2017

DOI: 10.1021/acs.jpcc.7b02727
J. Phys. Chem. C 2017, 121, 13008−13017

the fixed charge model only describes ionic bonds for fixed charge states in a simplified method. Therefore, previous studies[4−12] have been restricted only to a relatively simple modeling of specific materials (or structures).

For a practical modeling of a wider range of LIB cathode materials, many-body potentials coupled with the variable charge model are more appropriate, as mentioned earlier. For the variable charge model, the charge equilibration (Qeq) method developed by Rappe and Goddard[13] has been effectively used. Depending on how the many-body part is handled, one can think of a few candidate potential models: the ReaxFF,[14−16] the charge-optimized many-body (COMB) potential,[17,18] and the combination of a modified embedded atom method (MEAM) with Qeq.[19,20] Islam et al.[16] developed a reactive force field (ReaxFF) potential for the Li−S system and, using molecular dynamics (MD) simulations, provided insight into the behavior of sulfur-based cathode materials that are needed to develop lithium−sulfur batteries. To the best of our knowledge, there is no application of the ReaxFF and the COMB potential to lithium metal oxide systems. This is probably due to the fact that the formalism for ReaxFF and the COMB potential has been designed and applied primarily for covalent materials rather than metallic compounds. On the other hand, the combination of MEAM and Qeq can be more advantageous in developing interatomic potential for the lithium metal oxide systems, because it is well-known that MEAM is a robust potential model for metallic compounds. Nevertheless, there are still very few studies using this kind of potential model for LIB cathode materials. Kong et al.[19] developed a charge-transfer (CT) MEAM potential for the ternary Li−Mn−O system and predicted fundamental materials properties such as the charge states and redox potentials of Li_2MnO_3. Even though they report a wide range of materials properties calculated at 0 K, they do not report dynamic properties obtained using MD simulations at finite temperatures. Further, the applicability of the potential in subunary and binary systems has not been reported in sufficient detail. The applicability of an interatomic potential at finite temperatures is decisive for practical application of the potential to an investigation of dynamic behavior of materials. The applicability to subunary and binary systems is also important for robust applications of the potential to a wide range of materials phenomena, for example, the lithiation of manganese oxides.

In a situation in which a reliable interatomic potential is not well prepared, it is obviously necessary to develop a new interatomic potential covering multicomponent metal oxide systems in order to enable large-scale atomistic simulations for LIB cathode materials. The second-nearest-neighbor (2NN) MEAM,[21,22] one of the latest versions of MEAM,[23−25] has been applied to a wide range of materials, including metals, covalent elements, and their alloys. Especially, it has been successfully applied to essential metallic elements associated with LIB cathode materials, such as Li,[26] Co,[27] Mn,[28] Ni,[29] Al,[29] and some of their alloys. Recently, our group further extended the 2NNMEAM to cover multicomponent oxide compounds by combining it with the Qeq[13] concept (2NNMEAM+Qeq).[20] Special attention to the removal of known problems found in the original Qeq method has been considered in the implementation of the Qeq method to the 2NNMEAM. From this point of view, we believe that 2NNMEAM+Qeq can be one of the most suitable potential models for LIB cathode materials systems.

An interatomic potential database for relevant materials needs to be developed to investigate materials phenomena (diffusion, phase transition, defect formation, lithiation/delithiation, etc.) at the atomic-scale and to achieve the ultimate goal of searching for optimum materials. As a part of a long-term project to develop an interatomic potential database for LIB cathode materials systems, the objective of this study is to develop a potential for the ternary Li−Mn−O system (including binary Li−O, Mn−O, and Li−Mn systems) based on the 2NNMEAM+Qeq potential formalism. In addition, we also carry out Li diffusion simulations to confirm that the dynamic material phenomena in LIB cathode materials can be reliably described through MD simulation using the developed potential. A brief description of the formalism and the parameters of the potential model (2NNMEAM+Qeq) is given in section 2. Then, we report on the quality of the parametrization for the ternary Li−Mn−O system as well as for the binary Li−O, Mn−O, and Li−Mn systems in section 3, paying attention to the stability of the potentials at finite temperatures. Finally, in section 4, we show that MD simulation using the developed potential can be a powerful and effective tool to evaluate diffusion properties in LIB cathode materials.

2. 2NNMEAM+QEQ POTENTIAL FORMALISM AND PARAMETERS

In the 2NNMEAM+Qeq potential formalism,[20] the total energy of a system contains two energy terms—nonelectrostatic and electrostatic energy terms—as expressed in eq 1. The nonelectrostatic term is exactly identical to the existing 2NNMEAM potential formalism[21] and is independent from the electrostatic term (charges). The electrostatic term is a function of the atomic positions ($\mathbf{r}$) and charges ($\mathbf{q}$).

$$E^{\mathrm{Total}} = E^{\mathrm{MEAM}}(\mathbf{r}) + E^{\mathrm{ES}}(\mathbf{r},\mathbf{q}) \tag{1}$$

The MEAM energy is approximated as

$$E^{\mathrm{MEAM}} = \sum_i \left[F_i(\bar{\rho}_i) + \frac{1}{2}\sum_{j\neq i} S_{ij}\phi_{ij}(R_{ij}) \right] \tag{2}$$

where F_i is the embedding function, ρ_i is the background electron density at site i. S_{ij} and $\phi_{ij}(R_{ij})$ are the screening factor and the pair interaction between atoms i and j separated by a distance R_{ij}, respectively. The details in the expression of MEAM energy are beyond the scope of this paper, so readers are referred to the literature[21,22] or to the Supporting Information (SI) for more details.

The electrostatic energy is expressed as the sum of atomic energy E_i^{atom} (or penalty energy) and the Coulomb pair interaction V_{ij}^{Coul}

$$E^{\mathrm{ES}} = \sum_i E_i^{\mathrm{atom}}(q_i) + \sum_{i,j(i\neq j)} \frac{1}{2} V_{ij}^{\mathrm{Coul}}(q_i,q_j,R_{ij}) \tag{3}$$

where q_i is the charge state of atom i. The charge state of each atom depends on the local environment. According to the Qeq concept,[13] the equilibrium charge can be computed by minimizing the total electrostatic energy (eq 3) under the condition of charge conservation. The original Qeq uses a simple quadratic function for the atomic energy. This is probably because one can solve the minimization problem simply via a linear method when using the simple quadratic function. However, this often leads to the instability of charge

DOI: 10.1021/acs.jpcc.7b02727
J. Phys. Chem. C 2017, 121, 13008−13017

Table 1. 2NNMEAM+Qeq Parameters for Pure Li, Mn, and O; Li−Mn, Li−O, and Mn−O Pairs; and Li−Mn−O Triplet[a]

element	Li	Mn	O	i–j pair	Li−Mn	Li−O	Mn−O
reference	bcc	bcc	dimer	reference	b2	b1	b1
E_c (eV/atom)	1.65	2.90	2.56	E_c (eV/atom)	1.78	1.68	1.78
R_e (Å)	3.02	2.53	1.21	R_e (Å)	2.69	1.95	2.13
α	3.10	5.73	6.88	α	4.02	7.32	5.29
d_{rep}	0.05	0.00	0.00	d_{rep}	0.00	0.07	0.10
d_{att}	0.05	0.00	0.00	d_{att}	0.00	0.07	0.00
A	0.95	0.70	1.44	$C_{min}(i-j-i)$	0.20	1.00	4.00
$t^{(1)}$	2.30	4.00	0.10	$C_{min}(j-i-j)$	0.16	0.30	0.80
$t^{(2)}$	5.00	−3.00	0.11	$C_{min}(i-i-j)$	0.16	0.70	3.00
$t^{(3)}$	0.50	−4.00	0.00	$C_{min}(i-j-j)$	0.16	0.60	0.80
$\beta^{(0)}$	1.65	4.30	5.47	$C_{max}(i-j-i)$	2.00	1.55	5.00
$\beta^{(1)}$	1.00	1.00	5.30	$C_{max}(j-i-j)$	2.80	1.55	2.80
$\beta^{(2)}$	4.00	2.00	5.18	$C_{max}(i-i-j)$	2.80	1.35	4.00
$\beta^{(3)}$	1.00	6.50	5.57	$C_{max}(i-j-j)$	2.80	2.15	2.80
C_{min}	0.16	0.16	2.00	$\rho_0(j)/\rho_0(i)$	2.0	24.0	12.0
C_{max}	2.80	2.80	2.80	i–j–k triplet	Li−Mn−O		
χ^0 (eV/e)	−9.50	−5.12	10.11	$C_{min}(i-k-j)$	4.00		
J^0 (eV/e^2)	50.0	23.3	20.5	$C_{min}(i-j-k)$	0.20		
$\Delta E^{(2)}$ (eV)	50	10.0	5.63	$C_{min}(j-i-k)$	4.00		
$\Delta E^{(3)}$ (eV)	-	50	50	$C_{max}(i-k-j)$	5.00		
$\Delta E^{(4)}$ (eV)	-	-	-	$C_{max}(i-j-k)$	5.00		
ζ (Å^{-1})	10.0	1.52	2.39	$C_{max}(j-i-k)$	5.00		
Z (e)	0.00	0.91	0.00				

[a]2NNMEAM parameters (E_c, R_e, α, d_{rep}, d_{att}, A, $t^{(1)}$, $t^{(2)}$, $t^{(3)}$, $\beta^{(0)}$, $\beta^{(1)}$, $\beta^{(2)}$, $\beta^{(3)}$, C_{min}, C_{max}) for pure Li[26] and Mn[28] and all parameters for pure O[20] are as published in the literature. Qeq parameters (χ^0, J^0, $\Delta E^{(2)}$, $\Delta E^{(3)}$, $\Delta E^{(4)}$, ζ, Z) for Li and Mn and 2NNMEAM parameters for Li−Mn, Li−O, Mn−O, and Li−Mn−O were optimized in this study.

states beyond the limit due to insufficient penalty energy. In our model, to overcome the charge instability problem and simultaneously to keep the minimization problem linear, we introduce a quadratic spline function of q_i for the atomic energy. The Coulomb pair interaction is computed through the Coulomb integration between two density functions of the 1s-Slater orbital, as in Streitz and Mintmire.[30] It has been found that the conventional atom-based charge description, q_i, can raise unrealistic charge-transfers between two isolated atoms that are at long-range distances apart or between two different metal element atoms in binary alloys. Also, the minimization problem cannot be straightforward when using the concept of the atom-based charge, because the constraint condition of charge conservation should be considered externally. To avoid unrealistic charge-transfer and the constrained minimization problem, our potential formalism uses the concept of the split-charge,[31] $\overline{q}_{ji}$, which represents the charge flow from the covalently bonded neighbor atom j to the atom i. More details on the algorithms and mathematics for computing the equilibrium charge using our potential model can be found in ref 20 or in the SI of this paper.

Our potential model, 2NNMEAM+Qeq, has 15 MEAM parameters (E_c, R_e, α, A, $t^{(1)}$, $t^{(2)}$, $t^{(3)}$, $\beta^{(0)}$, $\beta^{(1)}$, $\beta^{(2)}$, $\beta^{(3)}$, C_{min}, C_{max}, d_{rep}, and d_{att}) and 7 Qeq parameters (χ^0, J^0, $\Delta E^{(2)}$, $E^{(3)}$, $E^{(4)}$, ζ, and Z) for each element. The Qeq part of our model operates only when a charge is assigned to the atoms in the system. This means that unary or metallic alloy systems are described only by the pristine 2NNMEAM formalism. Thus, we used the previously reported 2NNMEAM parameters of Li[26] and Mn[28] without any modification. The 2NNMEAM and Qeq parameters for pure O were taken from the previous work for the Ti−O and Si−O systems.[20] To describe the interaction between two different elements (i and j), the 2NNMEAM formalism requires 14 more parameters [ΔE_c, R_e, α, d_{rep}, d_{att}, $C_{min}(i-j-i)$, $C_{min}(j-i-j)$, $C_{min}(i-i-j)$, $C_{min}(i-j-j)$, $C_{max}(i-j-i)$, $C_{max}(j-i-j)$, $C_{max}(i-i-j)$, $C_{max}(i-j-j)$, and $\rho_0(i)/\rho_0(j)$]. These binary 2NNMEAM parameters for each metal−oxygen pair and Qeq parameters for each metallic element were optimized by fitting the fundamental physical properties of lithium oxides and manganese oxides. For a ternary system, six more parameters for the i–k–j triplet [$C_{min}(i-k-j)$, $C_{min}(i-j-k)$, $C_{min}(j-i-k)$, $C_{max}(i-k-j)$, $C_{max}(i-j-k)$, and $C_{max}(j-i-k)$] determine the screening effect of the k atom between the i–j pair. Therefore, a total of sixty-two parameters (7 Qeq parameters each for Li and Mn; 14 binary MEAM parameters each for Li−Mn, Li−O, and Mn−O; and 6 ternary MEAM parameters for Li−Mn−O) were optimized in this study.

To complete the ternary Li−Mn−O potential parameter set, we first optimize the Qeq parameters of the metal elements (Li and Mn) and the 2NNMEAM parameters of the metal−oxygen pairs (Li−O and Mn−O) by fitting the properties of each binary metal oxide system. After determining the Li−O and Mn−O binary potential parameters, we finally optimize the 2NNMEAM parameters for the binary Li−Mn and ternary Li−Mn−O systems by fitting the lithium manganese oxide properties. Since the properties of oxide systems are determined by combined effects of the MEAM and Qeq parts, the parameters from the two parts are optimized simultaneously. In case of the Li−Mn binary system, there is no stable compound to be considered for parameter optimization. Therefore, we first determine the E_c, R_e, α, d_{rep}, and d_{att} parameters of the Li−Mn pair by fitting the equation of state (EOS) for a given reference structure (B2 in this study) to DFT calculation. Then, the remaining 2NNMEAM parameters for the Li−Mn pair and those for the Li−Mn−O triplet are optimized by fitting the fundamental physical properties of the

DOI: 10.1021/acs.jpcc.7b02727
J. Phys. Chem. C 2017, 121, 13008−13017

Table 2. Lattice Parameters of Lithium Manganese Oxide Phases in Comparison with Experimental Data and DFT Calculation

phase		2NNMEAM+Qeq	% error	expt	DFT[k]	% error
spinel $LiMn_2O_4$	a (Å)	8.0669	−2.19	8.2474[a], 8.2483[b]	8.431	+2.22
layered Li_2MnO_3	a (Å)	4.7492	−3.73	4.9292[c], 4.937[d]	5.011	+1.58
	b (Å)	8.4564	−0.88	8.5315[c], 8.532[d]	8.633	+1.19
	c (Å)	4.7244	−6.03	5.0251[c], 5.030[d]	5.092	+1.28
	β (deg)	109.5610	+0.15	109.337[c], 109.46[d]	109.48	+0.07
layered $LiMnO_2$	a (Å)	4.7276	−13.02	5.431[e], 5.439[f]	5.488	+0.98
	b (Å)	2.7295	−2.83	2.809[e], 2.809[f]	2.872	+2.24
	c (Å)	4.9530	−8.15	5.390[e], 5.395[f]	5.395	+0.05
	β (deg)	108.5520	−6.36	115.95[e], 115.9[h]	115.412	−0.44
o-$LiMnO_2$	a (Å)	3.9093	−14.58	4.574[g], 4.5795[h]	4.634	+1.25
	b (Å)	5.6825	−1.41	5.752[g], 5.7750[h]	5.833	+1.21
	c (Å)	2.7342	−2.67	2.808[g], 2.8106[h]	2.869	+2.13
t-$LiMnO_2$	a (Å)	5.5688	−1.43	5.6488[i], 5.6504[j]	5.767	+2.08
	c (Å)	7.8755	−14.58	9.198[i], 9.242[j]	9.321	+1.1
rRMSE (%)			6.62			1.56

[a]Reference 32. [b]Reference 33. [c]Reference 34. [d]Reference 35. [e]Reference 36. [f]Reference 37. [g]Reference 38. [h]Reference 39. [i]Reference 40. [j]Reference 41. [k]Reference 42.

Table 3. Bulk Modulus (B) and Enthalpy of Formation (ΔH_f) of Lithium Manganese Oxide Phases in Comparison with DFT Calculation and Average Atomic Charges (q_{avg}) Assigned to Li, Mn, and O Atoms in Each Phase

	B (GPa)		ΔH_f (eV/atom)		q_{avg} (e)		
phase	2NNMEAM+Qeq	DFT[a]	2NNMEAM+Qeq	DFT[a]	Li	Mn	O
spinel $LiMn_2O_4$	147	112	−1.943	−2.033	+0.443	+0.890	−0.556
layered Li_2MnO_3	182	113	−2.087	−2.186	+0.425	+0.898	−0.583
layered $LiMnO_2$	217	112	−2.115	−2.156	+0.423	+0.855	−0.640
o-$LiMnO_2$	188	111	−2.114	−2.154	+0.422	+0.878	−0.638
t-$LiMnO_2$	150	113	−2.095	−2.156	+0.415	+0.856	−0.646

[a]Reference 42.

lithium manganese oxide compounds. The properties considered for fitting are lattice parameters, elastic constants, enthalpy of formation, and lithium migration energy barrier. The optimization of the parameters is performed using a genetic algorithm (GA). After obtaining several optimized parameter sets, we verify the reliability of the optimized parameter sets through simulations at finite temperatures and, then, finally select the most reliable set. The finally selected potential parameters are listed in Table 1.

3. EVALUATION OF THE DEVELOPED POTENTIALS

To obtain reasonable insight from the results of atomistic simulations, the interatomic potential should be accurate and well-verified for the system under consideration. Basically, a reliable interatomic potential should be able to correctly reproduce various fundamental physical properties (structural, elastic, thermodynamics, etc.) of the relevant materials. We calculate the fundamental physical properties of the Li−Mn, Li−O, Mn−O, and Li−Mn−O oxide compounds using the developed potentials and compare them with relevant experimental data and/or DFT calculations to evaluate the quality of the potential. To ensure the reproducibility of the potential for diffusion properties, we calculate the lithium migration energy barrier in anti-fluorite-type Li_2O and spinel-type $LiMn_2O_4$. The redox potential, which describes the voltage needed to extract lithium atoms out of the bulk system, is calculated to confirm that our potential reproduces the energetics of the charge/discharge process in cathode materials well. In addition, defect properties such as surface energy and point defect formation energy are calculated and compared with those from DFT calculations. We do not include the evaluation for Li−Mn, Li−O, and Mn−O binary systems in this section but present them in the SI and cover only the Li−Mn−O ternary system in this section.

For calculations, we use our own in-house code in which the 2NNMEAM+Qeq formalism is implemented. The code is provided as part of the SI of this paper. To obtain an equilibrium structure of various phases, the internal stresses in the initial samples are completely relaxed by allowing atomic movement and variation of cell size. At the initial step of the simulation, the equilibrium charges of individual atoms are first assigned by performing the Qeq. The Qeq process is performed at every 1000 steps rather than at every single step because it requires more expensive computational costs than do conventional energy calculations. We have confirmed that the calculation results are not significantly dependent on the frequency of the Qeq process. The cutoff distances for 2NNMEAM and Coulomb interaction are taken as 4.8 and 12.0 Å, respectively.

In the Li−Mn−O ternary system, spinel $LiMn_2O_4$ (space group $Fd\bar{3}m$[32,33]), layered Li_2MnO_3 (space group $C2/m$[34,35]), and layered $LiMnO_2$ (space group $C2/m$[36,37]) are of great interest as LIB cathode materials. There are two more polymorphs of $LiMnO_2$: orthorhombic (space group $Pmnm$[38,39]) and tetragonal (space group $I4_1/amd$[40,41]) structures. We compare the calculated fundamental physical properties (lattice parameters, elastic constants, and enthalpies of formation) of Li−Mn−O compounds with experimental data and/or DFT calculations. For practical applications, we check the reproducibility of the present potential for the lithium

DOI: 10.1021/acs.jpcc.7b02727
J. Phys. Chem. C 2017, 121, 13008−13017

migration energy barrier, redox potential, surface energy, and point defect formation energy. We also check the stability of the ternary compounds in MD simulations over a wide temperature range. Table 2 shows the calculated lattice parameters of lithium manganese oxide compounds in comparison with experimental data[32−41] and DFT calculation.[42] The present potential generally underestimates the lattice parameters compared to the experiments, and the relative root-mean-squared error (rRMSE) is 6.62%. The error is mainly generated from $LiMnO_2$ phases because more weight is given to the structural properties of spinel $LiMn_2O_4$ and layered Li_2MnO_3, which are more easily synthesized in experiments than are $LiMnO_2$ phases. Table 3 summarizes the calculated bulk modulus, enthalpy of formation, and average atomic charges in comparison with those from DFT calculation.[42] The present potential generally overestimates the bulk modulus compared to the DFT calculation. The calculated enthalpy of formation agrees well with that from the DFT calculation. The charge states of Li, Mn, and O in our calculation are somewhat lower than the formal charges. We do not consider the charge states of individual elements as a target property for fitting, but we obtain them as a result of the fitting to better reproduce other properties and to make the simulation stable. Too large charge values often cause the instability problem during the simulation. The energy contribution from the electrostatic Qeq part in the total energy of lithium manganese oxide system is about 60%, indicating that the charge transfer effect is sufficiently considered in our calculation. The properties mentioned next are calculated from samples including defects (thermal fluctuations and vacancies), and the charge states of individual atoms are automatically determined by the Qeq, depending on their neighboring environments. The electrostatic neutrality of the system is always maintained.

The diffusion properties of lithium have an important influence on the performance of LIB cathode materials. One of the main purposes of the present potential development for the Li−Mn−O system is to investigate the lithium diffusion properties in cathodes through large-scale atomistic simulations at finite temperatures. As a means to see if the present potential can predict the diffusion properties reasonably well through MD simulations, we calculate the lithium migration energy barrier in spinel $LiMn_2O_4$ at 0 K, in advance. In the spinel $LiMn_2O_4$ unit cell (space group $Fd\bar{3}m$), eight Li atoms occupy 8a sites, and there are interstitial sites at the 16c site between two adjacent 8a sites. It is known that lithium atoms migrate through the interstitial 16c site in the spinel $LiMn_2O_4$ lattice. To calculate the migration energy barrier, we calculate the relative energy as a lithium atom migrates from an initial 8a site to a neighboring vacant 8a site along a straight line. The movement of the lithium atom on the plane perpendicular to the migration direction is not allowed. The positions of the migrating lithium and a few distanced atoms are fixed and the positions of neighboring atoms and cell size are fully relaxed. To check the cell size effect in the calculation, we consider different cell sizes, including 55 (unit cell), 447 (2 × 2 × 2 super cell), and 3583 atoms (4 × 4 × 4 super cell). The size effect is negligible, as shown in Figure 1. The present potential predicts the migration energy barrier to be around 0.7 eV, and the saddle shape of the curves indicates that the barrier exists between the 8a site and the 16c site. Takai et al.[43] report a different activation energy of diffusion depending on the temperature range: 0.52 eV (at a lower temperature region, 300−600 °C), 1.11 eV (at a higher temperature region, 600−800 °C), and 0.77 eV (for the whole temperature region, 300−800 °C). The saddle shape of the activation energy curve is also reported by Verhoeven et al.,[44] with an activation energy value of 0.5 eV for jumping from an 8a to a 16c site, which is comparable to the low-temperature value of Takai et al. Xu and Meng[45] investigate the lithium migration energy barrier in spinel $LiMn_2O_4$ through a DFT calculation under different valence states of Mn ions and their arrangement, and they report calculated values within the range of 0.2−0.8 eV. Hoang[46] also reports the lithium migration energy barrier for different neighboring Mn charge states, in the range of 0.19−0.57 eV. According to our calculation, the charge state of all neighboring Mn atoms in the sample are the same due to the identical atomic environment of individual Mn sites. The present calculation for the lithium migration energy barrier agrees reasonably well with the reference data in the absolute value and also in the saddle shape of the energy curve.

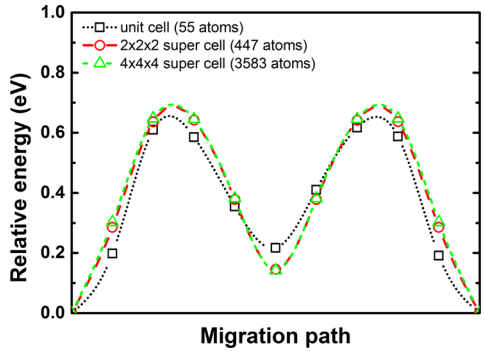

Figure 1. Relative energy as a lithium atom migrates in spinel $LiMn_2O_4$ along the migration path (Li 8a site → interstitial 16c site → vacancy 8a site). The present calculation predicts the migration energy barrier to be about 0.7 eV.

To check whether the present potential reproduces the redox reactions well during the charge/discharge process, we calculate the redox potential and compare it with the DFT calculations. We do not include the redox potential in the target property for the parameter optimization, but we intend to confirm that the parameter set fitted to the enthalpy of formation of lithium and oxides reproduces the redox potential well. The redox potential describes the voltage needed to extract Li atoms out of a bulk system. It can be computed using

$$\langle V \rangle = -\frac{G(\mathrm{Li}_{x_2}\mathrm{MO}) - G(\mathrm{Li}_{x_1}\mathrm{MO}) - (x_2 - x_1)G(\mathrm{Li})}{(x_2 - x_1)e} \quad (4)$$

where $G(X)$ is the Gibbs free energy of X, e is the elementary charge, and MO refers to the Mn_xO_y of the lithium manganese oxide compound. The Gibbs free energy can be replaced by the potential energy at 0 K, approximating the contribution of enthalpy (PV term) and entropy (TS term) to be negligible. Table 4 summarizes the calculated redox potential in comparison with experimental data[47,48] and DFT calculations[49,50] [generalized gradient approximation (GGA) and GGA+U]. It should be mentioned here that we calculated the redox potential for a wide range of Li compositions, for spinel $Li_xMn_2O_4$ ($0 < x < 1$) and layered Li_xMnO_3 ($1 < x < 2$). The redox potential is almost independent of the lithium composition, and only the average values are presented in Table 4. For spinel $LiMn_2O_4$, the calculated redox potential associated with full delithiation ($LiMn_2O_4/\lambda$-MnO_2), 3.47 V,

DOI: 10.1021/acs.jpcc.7b02727
J. Phys. Chem. C 2017, 121, 13008−13017

Table 4. Redox Potentials (V) in Spinel $LiMn_2O_4$ and Layered Li_2MnO_3 in Comparison with Experimental Data and GGA and GGA+*U* Calculations

phase	2NNMEAM +Qeq	expt	GGA	GGA+*U*
spinel $LiMn_2O_4$/λ-MnO_2	3.47	4.1[a]	3.37[c]	4.04[c]
layered Li_2MnO_3/$LiMnO_3$	3.58−3.80	4.4−5.0[b]	4.0−4.2[d]	4.5−4.9[d]

[a]Reference 47. [b]Reference 48. [c]Reference 49. [d]Reference 50.

somewhat underestimates the experimental value (4.1 V)[47] and the GGA+*U* calculation (4.04 V),[49] while being rather close to the GGA calculation (3.37 V).[49] Because Li ions can be extracted from different lithium sites (4h, 2c, and 2b) in the layered Li_2MnO_3 structure, the redox potential for layered Li_2MnO_3 is calculated from several configurations of delithiated $LiMnO_3$ according to the lithium vacancy distribution. We obtain the redox potential for layered Li_2MnO_3/$LiMnO_3$ in the range from 3.58 to 3.80 V. Experimentally, Li_2MnO_3 is believed to be responsible for the voltage range from 4.4 to 5.0 V.[48] The redox potential values from DFT calculations using GGA and GGA+*U* are 4.0−4.2 and 4.5−4.9 V, respectively.[50] As in the case of spinel $LiMn_2O_4$, the present potential underestimates the redox potential of the layered Li_2MnO_3 compared to the experimental value. GGA also generally underestimates the redox potential but can reproduce the value close to that of the experiments when adopting an optimal *U* value that contributes to the Coulomb interactions in the localized d or f orbitals in transition metals.[51] The difference in the redox potential between our calculation and GGA+*U* comes mainly from the difference in the potential energy of pure lithium between the calculation methods. We think it is meaningless to exactly reproduce the redox potential from GGA+*U* on the basis of the different description for the potential energy of pure lithium and do not include the redox potential in the fitting.

We also check whether the present potential reproduces the defect properties such as surface energy and point defect formation energy well. There are various surface structures of spinel $LiMn_2O_4$ depending on the orientation and termination. We prepare slab samples with the same surface structure on both sides by moving some of surface ions to the opposite surface, as described in the literature on DFT calculation.[52−54] We consider seven surface structures for the calculation of the surface energy, and Table 5 shows the calculated surface energies in comparison with the DFT calculations.[52−54] The present potential reproduces the surface energy and relative stability among surfaces of various structures fairly well. In order to calculate the point defect formation energy of spinel $LiMn_2O_4$, we consider point defects where the chemical composition formula does not change, that is, Frenkel and Schottky defects. The X Frenkel defect includes an X vacancy and an X interstitial defect (in a 16c site for the spinel structure), and we calculate the formation energy of the Frenkel defect depending on the relative distance between the vacancy and the interstitial defect (*isolated* or *neighboring*). The Schottky defect is the vacancies in stoichiometric units maintaining an overall neutral charge. We consider the Shottky defect by removing one Li, two Mn, and four O atoms in the spinel $LiMn_2O_4$ sample containing about 3000 atoms. Since there are many cases in selecting atoms to be removed, we select the atoms randomly and calculate the average energy from multiple trials. The calculated point defect formation energies are shown in Table 6, in comparison with another empirical model (the Born + shell model)[4] and a DFT calculation.[46] To the best of our knowledge, there is only one DFT calculation for the Li Frenkel. The DFT calculation is for the second-nearest-neighboring defect pair, which has a value similar to that of the *isolated* case according to our calculation. Our calculation is comparable to the DFT data[46] and also the other empirical data[4] for the Li Frenkel, while there are some discrepancies between our calculation and the other empirical calculation[4] for the other types of point defect.

Table 5. Surface Energy (J/m^2) of Spinel $LiMn_2O_4$ for Various Surface Structures in Comparison with DFT Calculations

surface structure (orientation−termination)	2NNMEAM +Qeq	DFT (GGA+*U*) ref52	ref53	ref54
(001)−Li_2	0.58	0.58	0.87	0.554
(001)−Mn_4O_8	0.93	0.98	1.28	1.199
(110)−$LiMnO_2$	0.88	0.99	1.39	1.233
(110)−MnO_2	0.85	1.19	1.52	1.162
(111)−Mn	0.63	0.85		0.834
(111)−Mn_3	1.98	1.29	1.18	1.682
(111)−O_4	1.31	1.30		1.201

Table 6. Formation Energies (eV) of Frenkel and Schottky Defects in Spinel $LiMn_2O_4$

defect	2NNMEAM +Qeq	empirical model[a]	DFT[b]
Li Frenkel (isolated/neighboring)	2.58/1.10	1.65	1.85
Mn Frenekel (isolated/neighboring)	2.39/2.62	6.27	
O Frenkel (isolated/neighboring)	3.73/3.91	6.69	
Schottky	8.56	5.03	

[a]Reference 4. [b]Reference 46.

According to our experience, so many potentials that perform well at 0 K often fail at finite temperatures. The representative example of this failure is a transformation of the structure into an unknown structure, with a decrease in the energy to a level that makes the unknown structure a stable phase on the phase diagram. In this case, one cannot use the potential for finite-temperature simulations, at least at the relevant compositional region. To check the applicability of the potential for finite-temperature simulations, we examine the energy and structural changes of all compound phases considered during heating and after cooling. The initial structure of each compound phase relaxed at 0 K is heated to 3000 K, increasing the temperature by 200 K and equilibrating the structure (containing 2000−4000 atoms) for 10 ps at each temperature with a Parrinello−Rahman *NpT* ensemble. Then, the structure heated to each temperature and rapidly cooled to 0 K is examined to determine whether the initial structure and energy have been recovered. From the recovery of the initial (0 K) structure and energy after rapid cooling, one can confirm that the potential does not generate undesirable structural changes during dynamic simulations (at finite temperatures). Figure 2 shows the change in internal energy of lithium

DOI: 10.1021/acs.jpcc.7b02727
J. Phys. Chem. C 2017, 121, 13008−13017

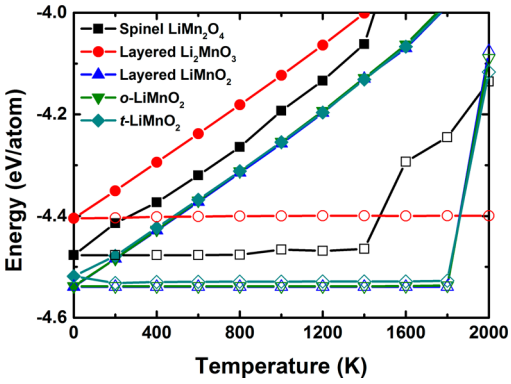

Figure 2. Change in energy of lithium manganese oxide phases as a function of temperature (solid symbols, during heating; open symbols, after rapid cooling to 0 K).

manganese oxide compounds as a function of temperature. The energy of all compounds monotonically increases during heating and recovers to the initial energy after rapid cooling to 0 K, which indicates that the present ternary potential is reliable for dynamic simulations in a wide temperature range and does not cause undesirable phase transformations (the appearance of an unknown structure as a stable phase).

4. DIFFUSION PROPERTIES OF LITHIUM IN SPINEL $LI_{1-X}MN_2O_4$

As mentioned previously, diffusion properties have a significant influence on the performance of LIB cathode materials. However, it has been restricted to measure the Li diffusion coefficient (D_{Li}) experimentally due to the nature of the very light element and no appropriate radioisotope for Li.[43] In addition, the effect of the stoichiometry on the diffusion properties during the charge/discharge process, in which the

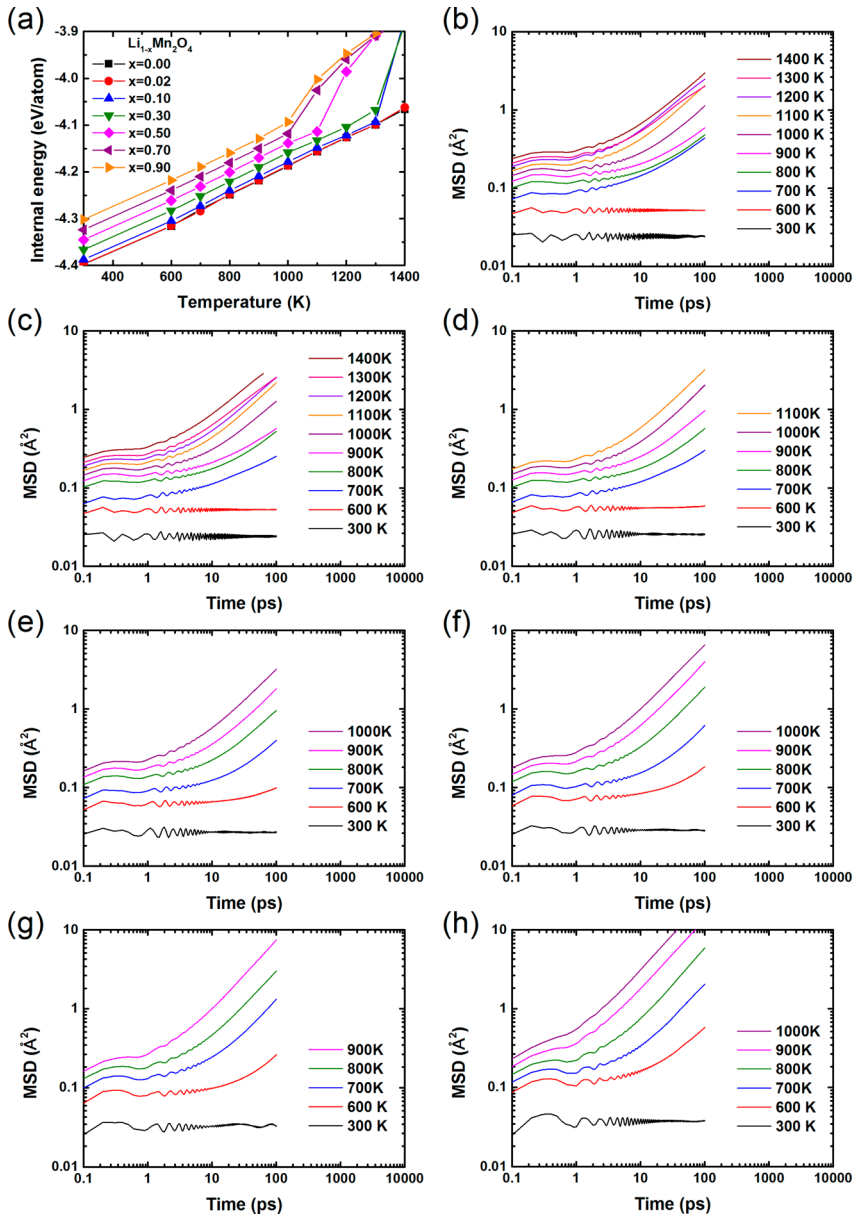

Figure 3. (a) Energy of spinel $Li_{1-x}Mn_2O_4$ as a function of temperature and mean-squared displacement (log scale) of lithium atoms in $Li_{1-x}Mn_2O_4$ as a function of time (log scale), where (b) $x = 0$, (c) $x = 0.02$, (d) $x = 0.1$, (e) $x = 0.3$, (f) $x = 0.5$, (g) $x = 0.7$, and (h) $x = 0.9$.

DOI: 10.1021/acs.jpcc.7b02727
J. Phys. Chem. C 2017, 121, 13008−13017

lithium vacancy concentration varies by the delithiation/lithiation, is not well-known experimentally and theoretically. Thus, we investigate the lithium diffusion properties in spinel $Li_{1-x}Mn_2O_4$ phases through MD simulations. We prepare a pristine spinel $LiMn_2O_4$ sample and randomly remove lithium atoms to obtain defective $Li_{1-x}Mn_2O_4$ samples containing about 1500 atoms, where x = 0.02, 0.1, 0.3, 0.5, 0.7, and 0.9. MD simulations are carried out at different temperatures (300−1400 K) for 10 ps for equilibration and another 1000 ps for analysis. Figure 3a shows the change in internal energy of the $Li_{1-x}Mn_2O_4$ sample as a function of temperature during the simulations. The $LiMn_2O_4$ phase maintains its structure up to 1400 K, as shown in Figures 3a and 2, and the temperature limit at which the structure of the defective $Li_{1-x}Mn_2O_4$ phase is maintained decreases as the lithium vacancy concentration increases.

We gather trajectories of samples at every 0.1 ps and calculate the mean-squared displacement (MSD) as

$$\mathrm{MSD} = \sum_{i=1}^{N} \frac{\langle |r_i(t) - r_i(0)|^2 \rangle}{N} \tag{5}$$

where $r_i(t)$ is the position vector of the lithium atom i at time t, N is the number of lithium atoms, and the angled brackets represent an ensemble average. To reduce statistical errors, the data for 1000 ps is divided into 10 parts, and the MSD values for individual 100 ps are averaged. We calculate the MSD of lithium atoms for each $Li_{1-x}Mn_2O_4$ sample (x = 0, 0.02, 0.1, 0.3, 0.5, 0.7 and 0.9) in a temperature range in which the structure is maintained. Figure 3b−h shows the calculated MSD as a function of time. The MSD curve is flat at temperatures below 600 K, because it is difficult to observe noticeable diffusion at low temperatures within a conventional MD simulation time scale. At temperatures above 600 K, the MSD linearly increases with time, which indicates the occurrence of lithium diffusion. As the temperature and the lithium vacancy concentration increase, the MSD increases more steeply, indicating that lithium atoms diffuse more easily.

For more quantitative analysis, we calculate the diffusion coefficient (D) of lithium using Einstein's relation

$$D = \frac{1}{2d} \lim_{t\to\infty} \frac{\mathrm{MSD}}{t} \tag{6}$$

where d is the dimension. In the spinel structure, lithium atoms can migrate through three-dimensional channels, and d is therefore 3. Figure 4 shows the calculated D_{Li} of $Li_{1-x}Mn_2O_4$ in the form of an Arrhenius plot. At low lithium vacancy concentrations, i.e., x = 0 and 0.02, the data points tend to deviate from a linear tendency, which is interpreted as a statistical error due to the lack of diffusion sites. As the lithium vacancy concentration increases, the data points are consistent with the linear tendency. At low temperatures below 600 K, the MSD curve is flat, as already mentioned, and D_{Li} cannot be obtained using eq 6. D_{Li} at an ambient temperature can be approximated by extrapolating high-temperature data. The estimated values for D_{Li} of spinel $Li_{1-x}Mn_2O_4$ at 300 K are within the range of 10^{-18}−10^{-16} m^2/s, as shown in Figure 4, where x varies from 0 to 0.9. The present calculation is in reasonable agreement with the experimental value[43], 1.3×10^{-18} m^2/s, obtained by the neutron radiography technique for $LiMn_2O_4$ samples.

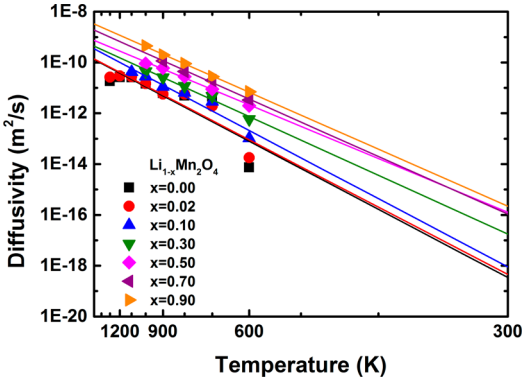

Figure 4. Diffusion coefficient (log scale) of lithium in spinel $Li_{1-x}Mn_2O_4$ as a function of temperature (reciprocal scale).

From the temperature dependency of the calculated D_{Li}, the activation energy (E_a) of lithium diffusion can be obtained through the following Arrhenius equation

$$D(T) = A \exp\left(-\frac{E_a}{k_B T}\right) \tag{7}$$

where T is the temperature, A is the pre-exponential factor, and k_B is the Boltzmann constant. Figure 5 shows the activation energy calculated as a function of the lithium vacancy concentration. Although data for low vacancy concentrations have a relatively high error range due to the statistical error in D_{Li}, the calculated values are in a range between 0.50 and 0.64 eV, which is in good agreement with the experimental values of 0.52−1.11 eV determined by Takai et al.[43] and 0.5 eV determined by Verhoeven et al.[44] One can expect that the activation energy obtained from the finite-temperature MD simulations may be lower than the migration energy barrier calculated at 0 K, since thermal fluctuations and vacancies in the lattice structure would facilitate the migration of lithium atoms. Indeed, the migration energy barrier obtained from the finite-temperature MD simulations, 0.50−0.64 eV, is slightly lower than the 0 K value, 0.7 eV.

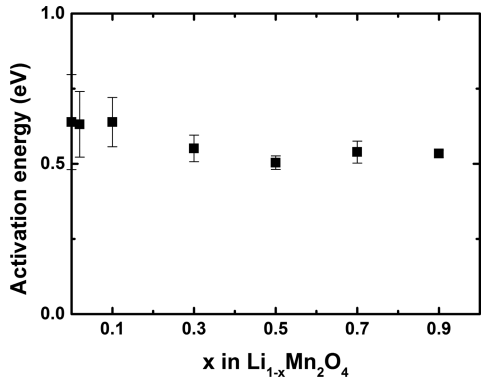

Figure 5. Activation energy for lithium diffusion in spinel $Li_{1-x}Mn_2O_4$ phases as a function of lithium vacancy concentration.

The calculated diffusion properties are self-consistent (showing a reasonable difference between finite-temperature values and the 0 K value of the migration energy barrier) and are in good agreement with the experimental data. We have found that the effect of lithium vacancy concentration is marginal on the activation energy for lithium diffusion in the $Li_{1-x}Mn_2O_4$ cathode, but it is significant on the lithium diffusion coefficient. However, it is necessary to mention about whether

DOI: 10.1021/acs.jpcc.7b02727
J. Phys. Chem. C 2017, 121, 13008−13017

our model describes the lithium diffusion based on an accurate physical principal. It is known that the lithium migration in oxide lattice structures is strongly influenced by a correlation effect of lithium ion and electron polaron.[46,55] Our model does not exclusively account for the polaron effect, and therefore, it may not be able to correctly reproduce the lithium diffusion properties. However, our model is based on a variable charge scheme, in which the lithium charge state is changed by the surrounding atomic environment as the lithium atom migrates. We hope and believe that the polaron effect is not completely neglected in our model.

Our ultimate goal is to analyze the effect of Mn, Co, and Ni composition on the lithium diffusion property, and we are developing Li−Co−O and Li−Ni−O potentials in a similar way. We believe that the approximation made for the polaron effect is applied similarly to each system, so that the potentials can be sufficiently utilized for large-scale atomistic simulations to predict the diffusion, phase transition, and defect properties of Li−(Co, Mn, Ni)−O multicomponent systems under various conditions of structure, composition, and alloying elements. The diffusion simulations described above can be carried out for Li−(Co, Mn, Ni)−O multicomponent systems in the iBat simulation platform (http://battery.vfab.org). iBat also provides various multiscale simulation techniques for LIB materials.

5. CONCLUSION

It has been shown that the 2NNMEAM+Qeq interatomic potential developed for the ternary Li−Mn−O system can describe various fundamental physical properties of lithium oxides, manganese oxides, and lithium manganese ternary oxides in reasonable agreement with relevant experimental data and/or DFT calculations. The lithium diffusion properties predicted by MD simulations based on this potential are self-consistent and match reasonably well with experiments. It is found that the lithium vacancy concentration has a significant influence on the lithium diffusion coefficient, while it has only marginal influence the activation energy for lithium diffusion. The developed Li−Mn−O potential can also be utilized for atomistic simulations on LIB cathode materials properties such as phase transitions, defect formation, and lithiation/delithiation. In addition, the potential can be further extended to multicomponent systems by combination with potentials for other Li−TM−O (TM: Co, Ni, etc.) systems and can be utilized for atomistic simulations on a wider range of LIB cathode materials.

■ ASSOCIATED CONTENT

Supporting Information

The Supporting Information is available free of charge on the ACS Publications website at DOI: 10.1021/acs.jpcc.7b02727.

Formalism of the 2NNMEAM and 2NNMEAM+Qeq interatomic potential models and the evaluation of binary potentials (Li−Mn, Li−O, and Mn−O) (PDF)

Source code for molecular dynamics simulation based on the 2NNMEAM+Qeq potential (ZIP)

■ AUTHOR INFORMATION

Corresponding Author

*E-mail: calphad@postech.ac.kr.

ORCID

Eunkoo Lee: 0000-0001-9159-2651

Notes

The authors declare no competing financial interest.

■ ACKNOWLEDGMENTS

This research was supported by the Industrial Strategic Technology Development Program (Grant No. 10041589), funded by the Ministry of Trade, Industry and Energy of Korea.

■ REFERENCES

(1) Mizushima, K.; Jones, P. C.; Wiseman, P. J.; Goodenough, J. B. Li_xCoO_2 ($0<x \leq 1$): A New Cathode Material for Batteries of High Energy Density. *Solid State Ionics* **1981**, *3−4*, 171−174.

(2) Doh, C.-H.; Kim, D.-H.; Kim, H.-S.; Shin, H.-M.; Jeong, Y.-D.; Moon, S.-I.; Jin, B.-S.; Eom, S.-W.; Kim, H.-S.; Kim, K.-W.; et al. Thermal and Electrochemical Behaviour of C/Li_xCoO_2 Cell during Safety Test. *J. Power Sources* **2008**, *175*, 881−885.

(3) Belov, D.; Yang, M.-H. Investigation of the Kinetic Mechanism in Overcharge Process for Li-Ion Battery. *Solid State Ionics* **2008**, *179*, 1816−1821.

(4) Ammundsen, B.; Rozière, J.; Islam, M. S. Atomistic Simulation Studies of Lithium and Proton Insertion in Spinel Lithium Manganates. *J. Phys. Chem. B* **1997**, *101*, 8156−8163.

(5) Kerisit, S.; Chaka, A. M.; Droubay, T. C.; Ilton, E. S. Shell Model for Atomistic Simulation of Lithium Diffusion in Mixed Mn/Ti Oxides. *J. Phys. Chem. C* **2014**, *118*, 24231−24239.

(6) Tealdi, C.; Spreafico, C.; Mustarelli, P. Lithium Diffusion in $Li_{1-x}FePO_4$: The Effect of Cationic Disorder. *J. Mater. Chem.* **2012**, *22*, 24870−24876.

(7) Lee, S.; Park, S. S. Structure, Defect Chemistry, and Lithium Transport Pathway of Lithium Transition Metal Pyrophosphates ($Li_2MP_2O_7$, M: Mn, Fe, and Co): Atomistic Simulation Study. *Chem. Mater.* **2012**, *24*, 3550−3557.

(8) Lee, S.; Park, S. S. Atomistic Simulation Study of Mixed-Metal Oxide ($LiNi_{1/3}Co_{1/3}Mn_{1/3}O_2$) Cathode Material for Lithium Ion Battery. *J. Phys. Chem. C* **2012**, *116*, 6484−6489.

(9) Sayle, T. X. T.; Caddeo, F.; Monama, N. O.; Kgatwane, K. M.; Ngoepe, P. E.; Sayle, D. C. Origin of Electrochemical Activity in Nano-Li_2MnO_3; Stabilization via a "Point Defect Scaffold. *Nanoscale* **2015**, *7*, 1167−1180.

(10) Tateishi, K.; Du Boulay, D.; Ishizawa, N. The Effect of Mixed Mn Valences on Li Migration in $LiMn_2O_4$ Spinel. A Molecular Dynamics Study. *Appl. Phys. Lett.* **2004**, *84*, 529−531.

(11) Lee, S.; Park, J.; Sastry, A. M.; Lu, W. Molecular Dynamics Simulations of SOC-Dependent Elasticity of $Li_xMn_2O_4$ Spinels in Li-Ion Batteries. *J. Electrochem. Soc.* **2013**, *160*, A968−A972.

(12) Fallahzadeh, R.; Farhadian, N. Molecular Dynamics Simulation of Lithium Ion Diffusion in $LiCoO_2$ Cathode Material. *Solid State Ionics* **2015**, *280*, 10−17.

(13) Rappe, A. K.; Goddard, W. A., III Charge Equilibration for Molecular Dynamics Simulations. *J. Phys. Chem.* **1991**, *95*, 3358−3363.

(14) van Duin, A. C. T.; Dasgupta, S.; Lorant, F.; Goddard, W. A., III ReaxFF: A Reactive Force Field for Hydrocarbons. *J. Phys. Chem. A* **2001**, *105*, 9396−9409.

(15) Senftle, T. P.; Hong, S.; Islam, M. M.; Kylasa, S. B.; Zheng, Y.; Shin, Y. K.; Junkermeier, C.; Engel-Herbert, R.; Janik, M. J.; Aktulga, H. M.; et al. The ReaxFF Reactive Force-Field: Development, Applications and Future Directions. *npj Comput. Mater.* **2016**, *2*, 15011.

(16) Islam, M. M.; Ostadhossein, A.; Borodin, O.; Yeates, A. T.; Tipton, W. W.; Hennig, R. G.; Kumar, N.; van Duin, A. C. T. ReaxFF Molecular Dynamics Simulations on Lithiated Sulfur Cathode Materials. *Phys. Chem. Chem. Phys.* **2015**, *17*, 3383−3393.

(17) Liang, T.; Shin, Y. K.; Cheng, Y.-T.; Yilmaz, D. E.; Vishnu, K. G.; Verners, O.; Zou, C.; Phillpot, S. R.; Sinnott, S. B.; van Duin, A. C. T. Reactive Potentials for Advanced Atomistic Simulations. *Annu. Rev. Mater. Res.* **2013**, *43*, 109−129.

(18) Liang, T.; Shan, T.-R.; Cheng, Y.-T.; Devine, B. D.; Noordhoek, M.; Li, Y.; Lu, Z.; Phillpot, S. R.; Sinnott, S. B. Classical Atomistic

Simulations of Surfaces and Heterogeneous Interfaces with the Charge-Optimized Many Body (COMB) Potentials. *Mater. Sci. Eng., R* **2013**, *74*, 255−279.
(19) Kong, F.; Zhang, H.; Longo, R. C.; Lee, B.; Yeon, D. H.; Yoon, J.; Park, J. H.; Doo, S. G.; Cho, K. A Large-Scale Simulation Method on Complex Ternary Li-Mn-O Compounds for Li-Ion Battery Cathode Materials. *Comput. Mater. Sci.* **2016**, *112*, 193−204.
(20) Lee, E.; Lee, K.-R.; Baskes, M. I.; Lee, B.-J. A Modified Embedded-Atom Method Interatomic Potential for Ionic Systems: 2NNMEAM+Qeq. *Phys. Rev. B: Condens. Matter Mater. Phys.* **2016**, *93*, 144110.
(21) Lee, B.-J.; Baskes, M. I. Second Nearest-Neighbor Modified Embedded-Atom-Method Potential. *Phys. Rev. B: Condens. Matter Mater. Phys.* **2000**, *62*, 8564−8567.
(22) Lee, B.-J.; Ko, W.-S.; Kim, H.-K.; Kim, E.-H. The Modified Embedded-Atom Method Interatomic Potentials and Recent Progress in Atomistic Simulations. *CALPHAD: Comput. Coupling Phase Diagrams Thermochem.* **2010**, *34*, 510−522.
(23) Baskes, M. I. Modified Embedded-Atom Potentials for Cubic Materials and Impurities. *Phys. Rev. B: Condens. Matter Mater. Phys.* **1992**, *46*, 2727−2742.
(24) Baskes, M. I.; Johnson, R. A. Modified Embedded Atom Potentials for HCP Metals. *Modell. Simul. Mater. Sci. Eng.* **1994**, *2*, 147−163.
(25) Baskes, M. I. Determination of Modified Embedded Atom Method Parameters for Nickel. *Mater. Chem. Phys.* **1997**, *50*, 152−158.
(26) Kim, Y.-M.; Jung, I.-H.; Lee, B.-J. Atomistic Modeling of Pure Li and Mg−Li System. *Modell. Simul. Mater. Sci. Eng.* **2012**, *20*, 035005.
(27) Dong, W.-P.; Kim, H.-K.; Ko, W.-S.; Lee, B.-M.; Lee, B.-J. Atomistic Modeling of Pure Co and Co-Al System. *CALPHAD: Comput. Coupling Phase Diagrams Thermochem.* **2012**, *38*, 7−16.
(28) Kim, Y.-M.; Shin, Y.-H.; Lee, B.-J. Modified Embedded-Atom Method Interatomic Potentials for Pure Mn and the Fe−Mn System. *Acta Mater.* **2009**, *57*, 474−482.
(29) Lee, B.-J.; Shim, J.-H.; Baskes, M. I. Semiempirical Atomic Potentials for the Fcc Metals Cu, Ag, Au, Ni, Pd, Pt, Al, and Pb Based on First and Second Nearest-Neighbor Modified Embedded Atom Method. *Phys. Rev. B: Condens. Matter Mater. Phys.* **2003**, *68*, 144112.
(30) Streitz, F. H.; Mintmire, J. W. Electrostatic Potential for Metal-Oxide Surfaces and Interfaces. *Phys. Rev. B: Condens. Matter Mater. Phys.* **1994**, *50*, 11996−12003.
(31) Nistor, R. A.; Polihronov, J. G.; Müser, M. H.; Mosey, N. J. A Generalization of the Charge Equilibration Method for Nonmetallic Materials. *J. Chem. Phys.* **2006**, *125*, 094108.
(32) Strobel, P.; Rousse, G.; Ibarra-Palos, A.; Masquelier, C. Disproportionation of Stoichiometric $LiMn_2O_4$ on Annealing in Oxygen. *J. Solid State Chem.* **2004**, *177*, 1−5.
(33) Akimoto, J.; Takahashi, Y.; Gotoh, Y.; Mizuta, S. Single Crystal Growth of the Spinel-Type $LiMn_2O_4$. *J. Cryst. Growth* **2001**, *229*, 405−408.
(34) Boulineau, A.; Croguennec, L.; Delmas, C.; Weill, F. Structure of Li_2MnO_3 with Different Degrees of Defects. *Solid State Ionics* **2010**, *180*, 1652−1659.
(35) Strobel, P.; Lambert-andron, B. Crystallographic and Magnetic Structure of Li_2MnO_3. *J. Solid State Chem.* **1988**, *75*, 90−98.
(36) Vitins, G.; West, K. Lithium Intercalation into Layered $LiMnO_2$. *J. Electrochem. Soc.* **1997**, *144*, 2587−2592.
(37) Capitaine, F.; Gravereau, P.; Delmas, C. A New Variety of $LiMnO_2$ with a Layered Structure. *Solid State Ionics* **1996**, *89*, 197−202.
(38) Akimoto, J.; Takahashi, Y.; Gotoh, Y.; Kawaguchi, K.; Dokko, K.; Uchida, I. Synthesis, Crystal Structure, and Magnetic Property of Delithiated Li_xMnO_2 ($x < 0.1$) Single Crystals: A Novel Disordered Rocksalt-Type Manganese Dioxide. *Chem. Mater.* **2003**, *15*, 2984−2990.
(39) Komaba, S.; Myung, S.-T.; Kumagai, N.; Kanouchi, T.; Oikawa, K.; Kamiyama, T. Hydrothermal Synthesis of High Crystalline Orthorhombic $LiMnO_2$ as a Cathode Material for Li-Ion Batteries. *Solid State Ionics* **2002**, *152−153*, 311−318.
(40) Wills, A. S.; Raju, N. P.; Morin, C.; Greedan, J. E. Two-Dimensional Short-Range Magnetic Order in the Tetragonal Spinel $Li_2Mn_2O_4$. *Chem. Mater.* **1999**, *11*, 1936−1941.
(41) Mosbah, A.; Verbaere, A.; Tournoux, M. Phase $Li_xMnO_2\lambda$ Rattachees Au Type Spinelle. *Mater. Res. Bull.* **1983**, *18*, 1375−1381.
(42) Jain, A.; Ong, S. P.; Hautier, G.; Chen, W.; Richards, W. D.; Dacek, S.; Cholia, S.; Gunter, D.; Skinner, D.; Ceder, G.; et al. Commentary: The Materials Project: A Materials Genome Approach to Accelerating Materials Innovation. *APL Mater.* **2013**, *1*, 011002.
(43) Takai, S.; Yoshioka, K.; Iikura, H.; Matsubayashi, M.; Yao, T.; Esaka, T. Tracer Diffusion Coefficients of Lithium Ion in $LiMn_2O_4$ Measured by Neutron Radiography. *Solid State Ionics* **2014**, *256*, 93−96.
(44) Verhoeven, V. W. J.; de Schepper, I. M.; Nachtegaal, G.; Kentgens, A. P. M.; Kelder, E. M.; Schoonman, J.; Mulder, F. M. Lithium Dynamics in $LiMn_2O_4$ Probed Directly by Two-Dimensional Li NMR. *Phys. Rev. Lett.* **2001**, *86*, 4314.
(45) Xu, B.; Meng, S. Factors Affecting Li Mobility in Spinel $LiMn_2O_4$-A First-Principles Study by GGA and GGA+U Methods. *J. Power Sources* **2010**, *195*, 4971−4976.
(46) Hoang, K. Understanding the Electronic and Ionic Conduction and Lithium over-Stoichiometry in $LiMn_2O_4$ Spinel. *J. Mater. Chem. A* **2014**, *2*, 18271−18280.
(47) Monge, M. Á.; Amarilla, J. M.; Gutiérrez-Puebla, E.; Campa, J. A.; Rasines, I. Atomic Level Study of $LiMn_2O_4$ as Electrode in Lithium Batteries. *ChemPhysChem* **2002**, *3*, 367−370.
(48) Yabuuchi, N.; Yoshii, K.; Myung, S.-T.; Nakai, I.; Komaba, S. Detailed Studies of a High-Capacity Electrode Material for Rechargeable Batteries, Li_2MnO_3−$nObu_{1/3}Ni_{1/3}Mn_{1/3}O_2$. *J. Am. Chem. Soc.* **2011**, *133*, 4404−4419.
(49) Chevrier, V. L.; Ong, S. P.; Armiento, R.; Chan, M. K. Y.; Ceder, G. Hybrid Density Functional Calculations of Redox Potentials and Formation Energies of Transition Metal Compounds. *Phys. Rev. B: Condens. Matter Mater. Phys.* **2010**, *82*, 075122.
(50) Chen, Y.-C.; Huo, M.; Liu, Y.; Chen, T.; Leng, C.-C.; Li, Q.; Sun, Z.-L.; Song, L.-J. Structural, Electrical, and Lithium Ion Dynamics of Li_2MnO_3 from Density Functional Theory. *Chin. Phys. Lett.* **2015**, *32*, 017102.
(51) Seo, D. H.; Urban, A.; Ceder, G. Calibrating Transition-Metal Energy Levels and Oxygen Bands in First-Principles Calculations: Accurate Prediction of Redox Potentials and Charge Transfer in Lithium Transition-Metal Oxides. *Phys. Rev. B: Condens. Matter Mater. Phys.* **2015**, *92*, 115118.
(52) Benedek, R.; Thackeray, M. M. Simulation of the Surface Structure of Lithium Manganese Oxide Spinel. *Phys. Rev. B: Condens. Matter Mater. Phys.* **2011**, *83*, 195439.
(53) Karim, A.; Fosse, S.; Persson, K. A. Surface Structure and Equilibrium Particle Shape of the $LiMn_2O_4$ Spinel from First-Principles Calculations. *Phys. Rev. B: Condens. Matter Mater. Phys.* **2013**, *87*, 075322.
(54) Lee, Y. K.; Park, J.; Lu, W. Electronic and Bonding Properties of $LiMn_2O_4$ Spinel with Different Surface Orientations and Doping Elements and Their Effects on Manganese Dissolution. *J. Electrochem. Soc.* **2016**, *163*, A1359−A1368.
(55) Kerisit, S.; Rosso, K. M.; Yang, Z.; Liu, J. Dynamics of Coupled Lithium/Electron Diffusion in TiO_2 Polymorphs. *J. Phys. Chem. C* **2009**, *113*, 20998−21007.

DOI: 10.1021/acs.jpcc.7b02727
J. Phys. Chem. C 2017, 121, 13008−13017